THE JOURNAL OF PHYSICAL CHEMISTRY B

Article

Cite This: J. Phys. Chem. B 2018, 122, 3079−3087

pubs.acs.org/JPCB

Operation of Kelvin Effect in the Activities of an Antifreeze Protein: A Molecular Dynamics Simulation Study

Uday Sankar Midya and Sanjoy Bandyopadhyay*

Molecular Modeling Laboratory, Department of Chemistry, Indian Institute of Technology, Kharagpur 721302, India

ABSTRACT: Ice growth and melting inhibition activities of antifreeze proteins (AFPs) are better explained by the adsorption-inhibition mechanism. Inhibition occurs as a result of the Kelvin effect induced by adsorbed protein molecules onto the surface of seed ice crystal. However, the Kelvin effect has not been explored by the state-of-the-art experimental techniques. In this work, atomistic molecular dynamics simulations have been carried out with *Tenebrio molitor* antifreeze protein (*Tm*AFP) placed at ice−water interface to probe the Kelvin effect in the mechanism of AFPs. Simulations show that, below equilibrium melting temperature, ice growth is inhibited through the convex ice−water interface formation toward the water phase and, above equilibrium melting temperature, ice melting is inhibited through the concave ice−water interface formation inward to ice phase. Simulations further reveal that the radius of curvature of the interface formed to stop the ice growth increases with decrease in the degree of supercooling. Our results are in qualitative agreement with the theoretical prediction of the Kelvin effect and thus reveal its operation in the activities of AFPs.

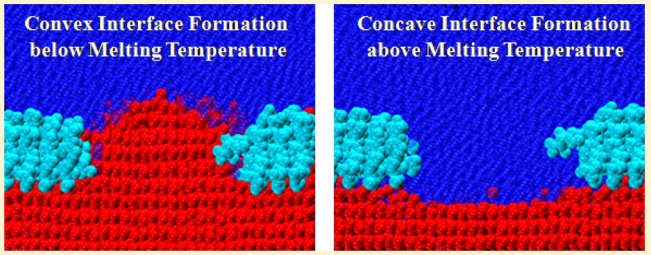

1. INTRODUCTION

Antifreeze proteins (AFPs) help certain fish,[1] insects,[2] plants,[3] and bacteria[4] to survive in harsh winter environments. AFPs inhibit the growth of ice and thus protect the species from the possible lethal effects of freezing at subzero temperatures. In the presence of AFPs, ice growth inhibition occurs due to the reduction of nonequilibrium freezing temperature of ice without appreciably affecting the equilibrium melting temperature. The difference between the two temperatures, termed as thermal hysteresis (TH), depends on not only the concentration but also the nature of the proteins. For example, small α-helical or globular AFPs present in polar fish[5,6] that belong to the moderately active AFP family show lower TH values.[7] On the other hand, relatively larger β-helical AFPs present in insects[8,9] belonging to the hyperactive AFP family exhibit higher TH values.[7] AFPs inhibit ice growth by using their unique ability of discriminating the solid phase of water, ice, from the large excess of liquid water, which help them to adsorb at the ice−water interface. The adsorbed protein molecules at the interface play an important role in the growth inhibition process. But how the growth inhibition occurs is not unambiguously understood. Even the adsorption of the proteins at the interface is itself debating. Several mechanisms assume reversible adsorption,[10−16] whereas few assume irreversible adsorption.[17−19] Although some experimental results support reversible adsorption,[20,21] fluorescence microscopy and microfluidic experiments[22,23] strongly suggest the irreversible adsorption, especially for hyperactive *Tenebrio molitor* AFP (*Tm*AFP).[8,24] The microfluidic experiment[23] even showed that the adsorbed protein molecules on a seed ice crystal are sufficient to exhibit thermal hysteresis irrespective of their presence in liquid phase surrounding the ice crystal. As mentioned by Knight and Wierzbicki,[19] irreversible adsorption seems to be reasonable, otherwise water molecules will occupy those ice lattice positions from where the protein molecules detach. Irreversible adsorption-based mechanism is therefore in action for antifreeze activity. The adsorption-inhibition mechanism proposed by Raymond and DeVries[17] is such type of mechanism mostly cited in the literature. According to this mechanism, action of AFPs below equilibrium melting temperature occurs in two steps. Adsorption of the protein molecules onto ice surfaces occurs first, followed by curved ice−water interface formation between the adsorbed protein molecules. As a result, local freezing temperature decreases according to the Kelvin effect[25] and hence ice growth is inhibited. However, the mechanism is not foolproof, as the operation of the Kelvin effect remains to be established. Wilson[12] pointed out for an experiment with a microscope of atomic resolution to explore the formation of curved interface and hence the Kelvin effect. Such experiment has not been performed to date by the state-of-the-art experimental techniques. Molecular dynamics (MD) simulations could, therefore, be useful for such purpose. Unfortunately, only a few simulations have been carried out to explore the Kelvin effect. The curved interface formation was shown by a statistical simulation technique.[26] But, in this simulation, reversible adsorption was considered and highly ideal interparticle interactions with no atomistic details were employed. Nada and Furukawa[27,28] carried out MD simulations with AFPs on ice−water interface. They showed that ice growth rate is

Received: January 25, 2018
Revised: February 28, 2018
Published: February 28, 2018

DOI: 10.1021/acs.jpcb.8b00846
J. Phys. Chem. B 2018, 122, 3079−3087

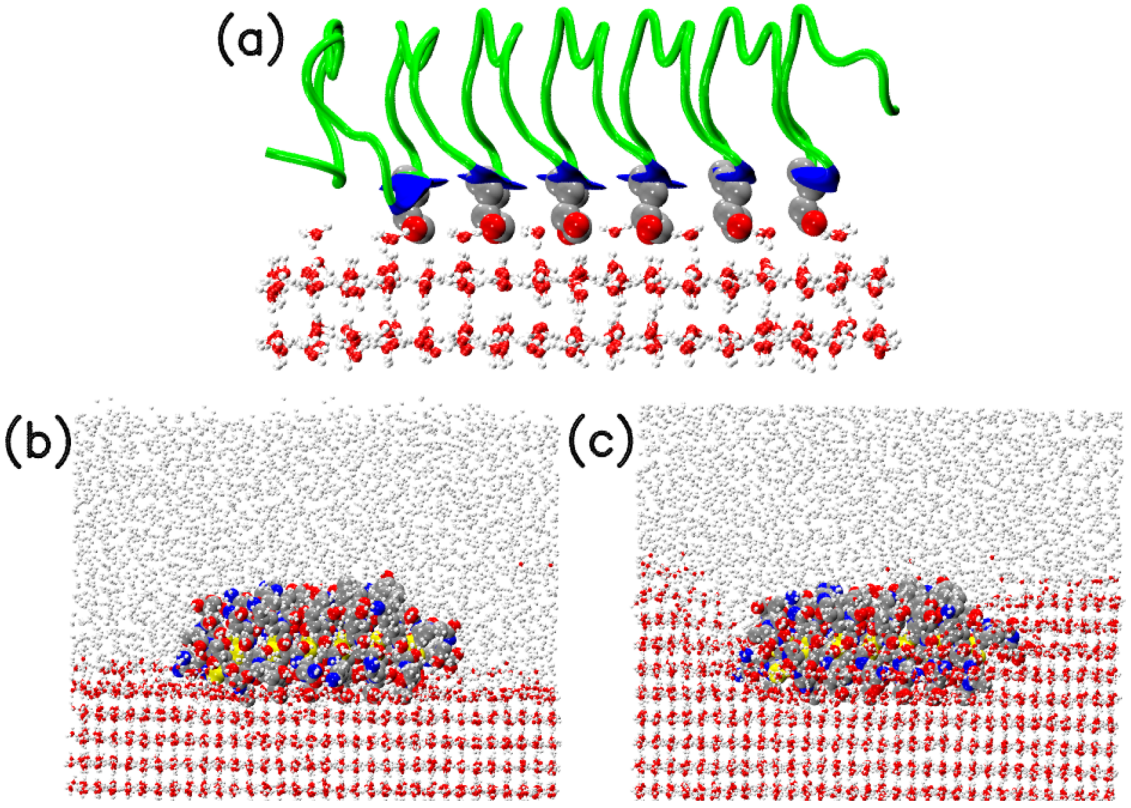

Figure 1. (a) Crystal structure of the *Tm*AFP protein[8] (drawn as cartoons) with employed interfacial water arrangement. IBS of the protein is drawn in blue, whereas the NIBS is drawn in green. Side chains of the threonine (T) residues in the IBS are drawn as spheres. Interfacial waters are drawn as balls and sticks. Starting configurations for (b) S1 and S2 simulations at 220 and 225 K, respectively, and (c) S3 simulation at 230 K. Protein is drawn as spheres, ice water molecules are drawn as balls and sticks, and liquid water molecules are drawn as white balls.

reduced at ice surface when the AFPs stably bound to the surface. However, cessation of ice growth does not occur, whereas growth is supposed to be stopped by the Kelvin effect. Recent simulations showed that local melting of ice around AFPs, which are not stably bound to ice, induces curved ice−water interface formation for inhibition of ice growth.[29,30] Apparently, no consensus notion exists regarding the action of the Kelvin effect in the mechanism of antifreeze activity, and such effect needs to be explored.

According to the Kelvin effect,[25] cessation of ice growth occurs due to the formation of convex interface toward the liquid phase. The critical radius, r^*, of the interface that would allow and restrict further growth at a temperature, T, within the hysteresis gap is given by[31]

$$r^* = \frac{2\sigma T_m}{\Delta H \Delta T} \quad (1)$$

where σ is the interfacial tension, T_m is the equilibrium melting temperature, ΔH is the latent heat of fusion, and ΔT is the degree of supercooling ($\Delta T = T_m - T$). Equation 1 suggests that regardless of the separation between the protein molecules on an ice plane the critical radius of the curved interface will decrease with increase in the degree of supercooling. As the degree of supercooling increases with the decrease in temperature below T_m, critical radius will therefore decrease with the decrease in temperature below T_m. Equation 1 further implies that if a convex interface is sustained to a higher temperature than that at which it is formed (i.e., sustained to a reduced degree of supercooling) the critical radius will increase by melting. Melting will continue until and unless the critical radius at the said supercooling is attained. If the sustained temperature is above T_m, there will be a possibility of melting inhibition with the formation of concave interface inward the ice phase (r^* is negative as ΔT is negative at $T > T_m$). AFPs indeed inhibit the melting of ice up to a certain temperature above T_m,[32−34] although the melting inhibition potential of an AFP is much more less than its growth inhibition potential. So, to establish the Kelvin effect in the mechanism of AFPs, it is required to examine, at least qualitatively, the cessation of ice growth and melting as well as change of interfacial radius with temperature. Such aspects have been studied in this work by means of atomistic MD simulations with a paradigm protein *Tm*AFP placed at the ice−water interface. The rest of the article has been organized as follows. In Section 2, we provide a brief description of the system setups and the simulation methods employed. The results obtained from our analyses are presented and discussed in Section 3. Finally, the important findings from the study and the conclusions reached therefrom are highlighted in Section 4.

2. SIMULATION DETAILS

We have carried out three simulations, designated as S1, S2, and S3, with the protein *Tm*AFP placed at the ice−water interface at three different temperatures, 220, 225, and 230 K, respectively. The initial coordinates of the protein were taken from its crystal structure (PDB code: 1EZG).[8] The 84-residue pseudo-rectangular-shaped right-handed β-helical *Tm*AFP contains 7 loops with a series of 12 residue repeats of sequence TCTxSxxCxxAx. The flat β-sheet formed by the threonine−cysteine−threonine (TCT) motifs of the loops (except the N-

DOI: 10.1021/acs.jpcb.8b00846
J. Phys. Chem. B 2018, 122, 3079−3087

terminal loop) is the ice-binding surface (IBS) of the protein. The remaining part of the protein is denoted as the nonice-binding surface (NIBS). The initial structure of the protein with employed protein−ice interfacial water arrangement is shown in Figure 1a. Prior to simulations, required modifications in the protein structure were done, as reported in our previous study.[35] The simulations were performed using the NAMD code.[36] The energy-minimized structure of the protein was placed at the ice−water interface. We created the ice−water interface on the basal plane of ice. IBS of the protein was in contact with the basal plane of ice. It may be noted that the basal plane was chosen as it is known that an hyperactive protein like *Tm*AFP preferentially binds to the basal plane of ice.[7,37] Protein−ice interfacial water arrangement was adopted to that we have reported previously.[38] To avoid unfavorable contacts, the protein was inserted at the flat interface by carefully removing the water molecules within 2 Å from any protein atom. Two Na^+ ions were added in liquid water to neutralize the whole system. Finally, the system contained the protein molecules in an orthorhombic cell with dimension 72.32 Å × 54.81 Å × 76.62 Å containing 3372 ice water molecules, 5376 liquid water molecules, and 2 Na^+ counterions. Three-tier energy minimization was done with the system using the conjugate gradient energy minimization method as implemented in the NAMD code:[36] first, by keeping all of the heavy atoms of the protein and the oxygen atoms of the ice water molecules constrained in their positions; second, by keeping only the backbone heavy atoms of the protein constrained in their positions; and finally, by removing all of the constraints. The system was then heated to 300 K within a short MD run of 100 ps under constant temperature and volume (NVT) condition. To equilibrate the ice−water interface, a 2 ns simulation under NVT condition was carried out at 300 K, keeping all backbone heavy atoms and the ice oxygen atoms constrained into their positions. The final configuration of this short run was used as the starting configuration for the S1 and S2 simulations at 220 and 225 K, respectively. The configuration is shown in Figure 1b. Temperatures were lowered to the respective target values and then at each of the temperatures the simulations were carried out for 300 ns under NVT condition. It is important to note that we have determined the melting point (T_m) of ice at the basal plane for TIP4P water by performing direct coexistence simulations of ice−water interface. Ice was found to continuously grow below 229 K and melt above 229 K, and the two phases remained stable at 229 K. Thus, considering the T_m of TIP4P water model to be 229 K, S1 and S2 simulations were carried out below T_m. During these simulations, we have employed much larger box length along the *z*-axis than the actual length of 76.62 Å to obstruct the ice growth on the protein-free ice−water interface that would otherwise exist under the employed periodic boundary conditions (PBCs).[39] After 300 ns run, condition of S1 simulation was changed from NVT to that of isothermal−isobaric ensemble (NPT) at constant pressure of 1 atm and constant temperature of 220 K. Change of simulation condition creates protein-free ice−water interface by eliminating the water−vacuum and ice−vacuum interfaces present in earlier stage. Simulation was performed for 20 ns to freeze those quasi-ice-like water molecules, which were present earlier in ice−vacuum interface. Final configuration, shown in Figure 1c, of this short 20 ns NPT run was used for the S3 simulation at 230 K. Temperature in S3 simulation was increased from 220 to 230 K at a heating rate of 1 K/ps. The simulation was then carried out at 230 K temperature for 300 ns under NPT ensemble condition. As the simulation temperature in S3 simulation is above the T_m of water model employed, ice could melt on either of the two ice−water interfaces (one contains *Tm*AFP and another free from *Tm*AFP). To stop the melting at the protein-free interface, the oxygen atoms of the closest hexagonal bilayer of ice on that interface were constrained to their initial positions. All simulations were carried out with an integration time step of 1 fs, whereas the trajectories were stored with a time resolution of 500 fs for subsequent analyses. All bonds involving the hydrogen atoms were constrained by the SHAKE algorithm.[40] The PBC and the minimum image convention[39] were employed to calculate the short-range Lennard-Jones interactions with a spherical cutoff distance of 12 Å and a switch distance of 10 Å. The long-range electrostatic interactions were calculated using the particle-mesh Ewald method.[41] The all-atom CHARMM22 force field and potential parameters for proteins with CMAP corrections[42,43] and TIP4P model[44] for water were employed in the simulations. It can be noted that the calculated T_m of TIP4P water model is in very good agreement with the other values reported in the literature.[45−48]

In all of the simulations, we have used only one *Tm*AFP molecule on the ice plane. But at least two molecules for curved step[17] or three molecules for bulge interface[15,19] formation are required to exhibit the Kelvin effect in between the protein molecules. This requirement is satisfied by the employed PBC in simulations. PBC generate an infinitely large rectangular array of the proteins on an infinitely large and flat ice surface, thus making it possible to detect the Kelvin effect using a single *Tm*AFP molecule.

3. RESULTS AND DISCUSSION

Permanent attachment (irreversible binding) of the protein onto the ice surface is the primary requirement for the exhibition of the Kelvin effect. In the simulations, protein is initially taken as in ice-bound state. So, it is required to

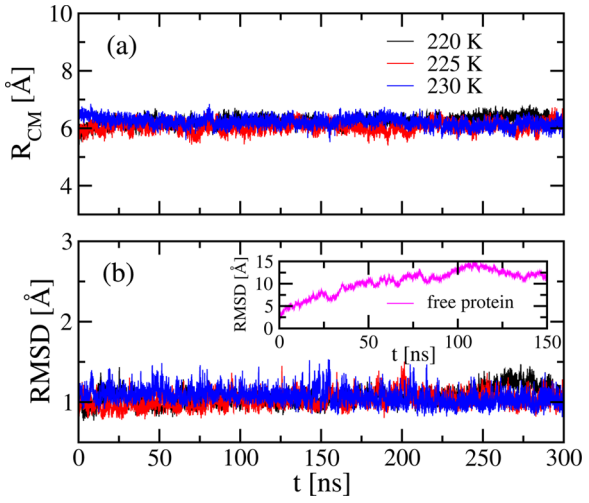

Figure 2. Time evolutions of (a) R_{CM}'s of *Tm*AFP with respect to ice surface and (b) RMSDs based on the nonhydrogen atoms of the *Tm*AFP protein (except two end residues from each terminal) with respect to the starting configuration of the protein as obtained from simulations S1 at 220 K, S2 at 225 K, and S3 at 230 K. Time evolution of RMSD obtained from our earlier simulation[35] of free protein in aqueous solution at 220 K is shown in the inset.

DOI: 10.1021/acs.jpcb.8b00846
J. Phys. Chem. B 2018, 122, 3079−3087

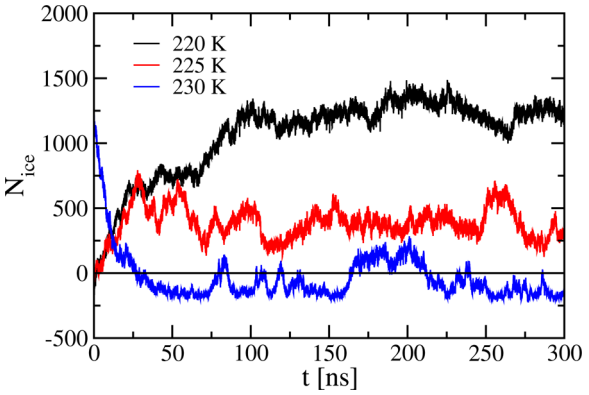

Figure 3. Time evolutions of the number of ice water molecules, N_{ice}, formed above the reference plane, $z = -4$, as obtained from simulations S1 at 220 K, S2 at 225 K, and S3 at 230 K. The negative values represent the appearance of liquid water molecules just below the reference plane.

Table 1. Average Number of Ice Water Molecules above the Reference Plane, $z = -4$, Present after 100 ns Onward as Obtained from Simulations S1 at 220 K, S2 at 225 K, and S3 at 230 K[a]

simulation	ice water molecules
S1	1237.3 (82.5)
S2	376.0 (101.8)
S3	−59.0 (113.4)

[a]The negative value represents the appearance of liquid water molecule just below the reference plane. The values in the parentheses are the corresponding standard deviations.

examine, prior to probing the ice growth or melting inhibition, whether such state remains intact during the course of simulations. It is visualized over the trajectory of each system that the protein indeed remains bound to the ice surface at all of the three temperatures. Quantitatively, we explore the intact nature by calculating the center of mass distance (R_{CM}) of the protein molecule with respect to ice surface. Variations of R_{CM} with time at three temperatures are displayed in Figure 2a. The distance remains unchanged as the simulations progresses, indicating that the protein remains bound onto the ice surface. However, the R_{CM} calculation does not reveal that the IBS of the protein is always in contact with ice because the cylindrical protein molecule can rotate when it is bound to a large ice surface. To ascertain whether the IBS is in contact with the ice surface, we probe the rotational motion of the protein molecule by calculating the root-mean-square deviations (RMSDs) of the simulated protein configurations with respect to the starting configuration. In traditional calculation of root-mean-square deviations, translational as well as rotational motions of macromolecules are eliminated, and such calculation reveals the conformational fluctuations of the molecules. In our calculation, we have not eliminated rotational motion. Therefore, in the present case, time evolution of RMSD values probe the rotational motion of the protein molecule. Calculations are carried out over all of the nonhydrogen atoms of the protein except two end residues from each of the terminals. Time evaluations of the RMSD values for the protein at three temperatures are shown in Figure 2b. For comparison, corresponding data from our earlier simulation of the free protein in solution at 220 K[35] are also shown in the inset. It can be seen that the protein at the interface exhibits very low RMSD values at all three temperatures, as compared to that in free state at 220 K. Such low RMSD values reveal that the rotational motion of the protein is completely frozen. Frozen rotational motion is also apparent from the observed variation of RMSD values of the protein at interface compared to that in solution. RMSD of the protein on ice surface remains unchanged, whereas in free state it changes continuously (inset in Figure 2b). As the IBS of the protein is initially in contact with ice, the frozen rotational motion indicates that the IBS remains in contact with the ice during the simulations. Moreover, frozen rotational motion of the large cylindrical protein molecule exhibits its perfect registration on ice surface possibly through the formation of hydrogen bonds between regularly arranged Thr hydroxyl groups on the IBS of the protein and periodically arranged water molecules on ice surface. The calculated number of hydrogen bonds formed by each Thr hydroxyl group on IBS with ice water molecules suggests that kind of registration. On average, each Thr hydroxyl group on the IBS forms 2.57 hydrogen bonds, close to its limiting value 3.00. Clearly, the results reveal that the protein is permanently bound onto the ice surface. Such binding may help the protein to exhibit the freezing and melting inhibition of ice.

Once the protein is bound onto the ice surface, the adsorption-inhibition mechanism requires that the ice will grow or melt, depending on the sustained temperature, in the open area of the surface.[17,32] If the temperature is in the active range of the protein, growth or melting will be ceased after attaining the corresponding critical radius as in eq 1. Such growth or melting could be detected by calculating the number of ice water molecules with time. A suitable order parameter is therefore needed to distinguish ice water molecules from liquid water molecules. The order parameter $\langle q_6 \rangle$ derived from Steinhardt order parameters[49] is the one that has been used previously.[38,50,51] $\langle q_6 \rangle$ is defined as

$$\langle q_6(i) \rangle = \left[\frac{4\pi}{13} \sum_{m=-6}^{6} |\langle q_{6m}(i) \rangle|^2 \right]^{1/2} \tag{2}$$

where

$$\langle q_{6m}(i) \rangle = \frac{1}{N_{ng} + 1} \sum_{j=0}^{N_{ng}} q_{6m}(j) \tag{3}$$

and

$$q_{6m}(i) = \frac{1}{N_{ng}} \sum_{j=1}^{N_{ng}} Y_{6m}(\theta_{ij}, \varphi_{ij}) \tag{4}$$

$Y_{6m}(\theta_{ij}, \varphi_{ij})$ is the sixth-order spherical harmonics, and θ_{ij} and φ_{ij} are the polar angles of the bond vector connecting i water molecule to the jth member of its N_{ng} number of neighboring molecules. Angles are measured in an external reference frame. Summation in eq 3 runs over all of the neighbors of i water molecule, including the molecule itself (when $j = 0$). In the calculation, we have considered only second-shell neighbors of a tagged water molecule to clearly identify it as an ice water molecule or liquid water molecule. From the $\langle q_6 \rangle$ distribution curves of pure water, pure ice, and ice−water coexisting system, we observed in our earlier study[38] that water molecules with $\langle q_6 \rangle$ value greater than 0.17 are ice water molecules. This cutoff value is also used here to identify ice water molecules. Change in the numbers of ice water molecules above $z = -4$ plane at

DOI: 10.1021/acs.jpcb.8b00846
J. Phys. Chem. B 2018, 122, 3079−3087

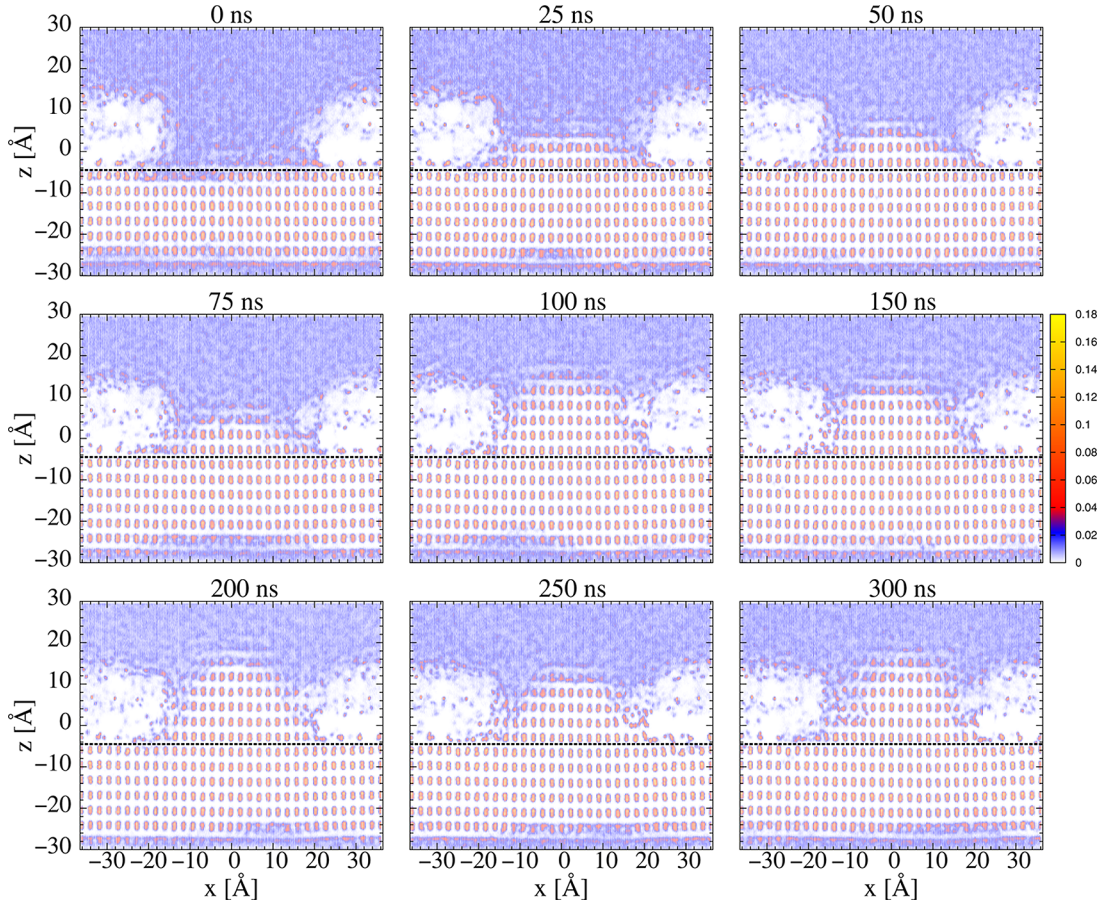

Figure 4. Two-dimensional probability distributions of water molecules around the *Tm*AFP protein on the *xz* plane (the protein helical axis is aligned along the *x* axis) as obtained at 0, 25, 50, 75, 100, 150, 200, 250, and 300 ns from simulation S1 at 220 K. In each panel, the reference plane, $z = -4$, is drawn as a black dashed line.

three temperatures is shown in Figure 3. The plane (henceforth used as "reference plane") is defined by setting the centroid of the protein as the origin of the Cartesian coordinate system. This plane is chosen as reference plane because, in the starting configuration (Figure 1b) used for the S1 and S2 simulations, the plane separates the flat ice surface from the liquid phase. The number of ice water molecules above the reference plane is calculated only to trace the change at the ice−water interface containing the protein molecule. The negative number of ice water molecules in the figure indicates the presence of liquid water molecules just beneath the reference plane. Figure 3 shows that the number of ice water molecules initially increases at 220 and 225 K but decreases at 230 K. After certain time, no further increase or decrease occurs, rather the numbers fluctuate around fixed values. Initial increase below T_m (i.e., at 220 and 225 K) and decrease above T_m (i.e., at 230 K) clearly suggest the growth and melting of ice, respectively. No further increase or decrease suggests the cessation of ice growth or melting. Importantly, the fluctuating numbers indicates that, although the growth or melting is ceased, the ice−water interface is not static rather dynamic. After cessation, some extent of ice formation and subsequent breaking of the same often occurs. The dynamic interface has also been observed in statistical simulation[26] and may be correlated to protein-induced long-range water dynamics.[52,53] The average number of newly formed ice water molecules above the reference plane and the average number of liquid water molecules just beneath the reference plane at the three temperatures are given in Table 1. The averages are calculated after 100 ns onward to exclude the initial growth or melting periods. The number of ice water molecules above the reference plane increases with the decrease of temperature. The presence of ice water molecules above the reference plane also indicates the formation of convex ice−water interface at 220 and 225 K, and the presence of liquid water molecules just beneath the reference plane indicates the formation of concave ice−water interface at 230 K. The formation of convex and concave interfaces can be better understood from the two-dimensional probability distributions of waters around the protein molecules. For the calculation of the distributions, the coordinates of all of the atoms are transformed in such a way that the helical axis of the protein remains aligned along the *x* axis, and the IBS remains parallel to the *xy* plane. Distributions are computed within a slice of the systems for better visualization of the interfaces. The slice containing part of the protein molecule is selected by setting the limit $-10.0 \leq y \leq 10.0$ Å. All water molecules within the slice are mapped on the *xz* plane (perpendicular to *y* axis and IBS). All waters are translated in between the protein molecule and PBC-generated first virtual image of the protein along the $+x$ direction. The distributions are calculated over a window of 2 ns at different time intervals. The window spans 1 ns each on either side of a time interval. The results obtained at 220, 225, and 230 K are shown in Figures 4−6, respectively. The black horizontal lines in the figures represent the reference plane. The regions in the figures with highly intense peaks correspond to the ice phase, and the low-intensity regions correspond to

DOI: 10.1021/acs.jpcb.8b00846
J. Phys. Chem. B 2018, 122, 3079−3087

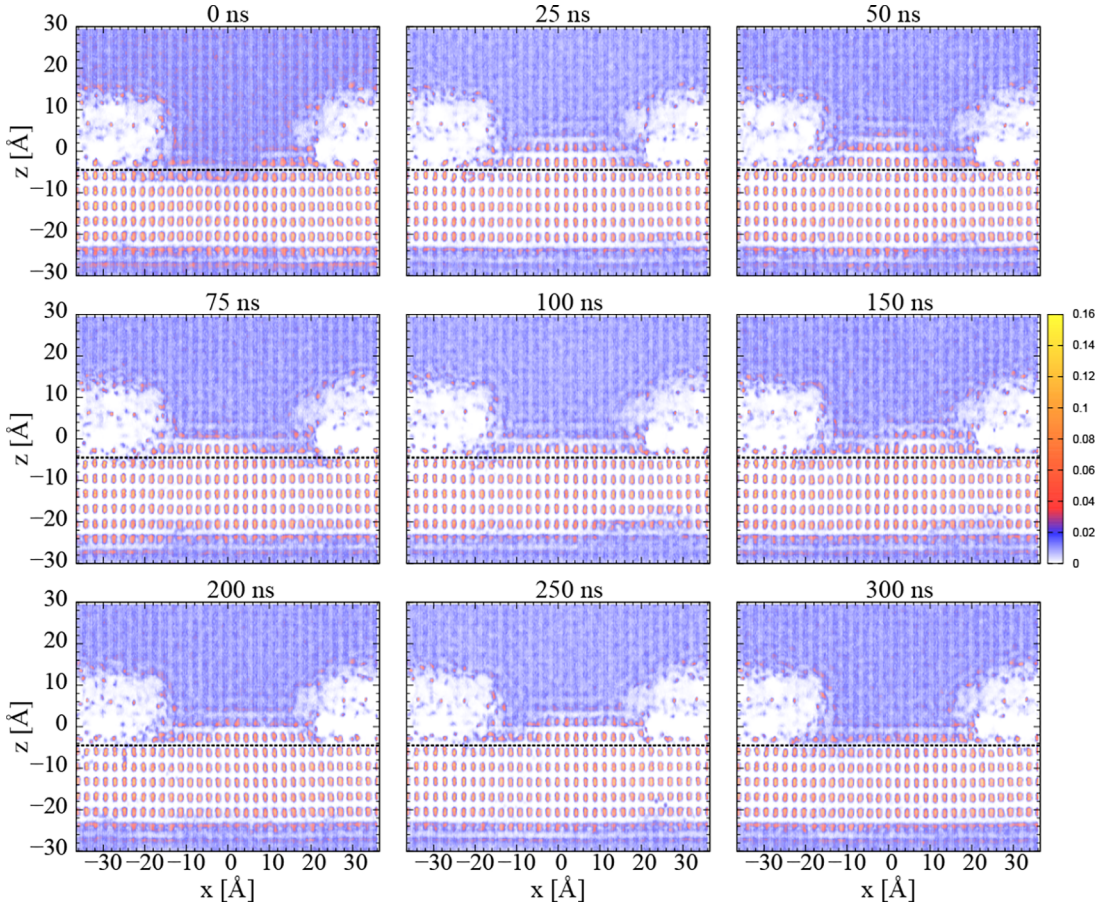

Figure 5. Two-dimensional probability distributions of water molecules around the *Tm*AFP protein on the *xz* plane (the protein helical axis is aligned along the *x* axis) as obtained at 0, 25, 50, 75, 100, 150, 200, 250, and 300 ns from simulation S2 at 225 K. In each panel, the reference plane, $z = -4$, is drawn as a black dashed line.

the liquid phase. It can be seen from Figure 4 that, at 220 K, ice grows up to 100 ns, and afterward no notable change appears. Same things occur at 225 K, as evident from Figure 5. However, ice grows only up to 25 ns at 225 K. It is apparent that the protein allows an initial growth of ice before complete inhibition of the growth. The growth is observed on the uncovered area of the ice surface. The amount of ice phase above the reference plane is greater at 220 K than that at 225 K. This correlates with the results presented in the previous section, where it was shown that the number of newly formed ice water molecules increases with decreasing the temperature below T_m. Figures 4 and 5 clearly reveal that the growth of ice leads to the formation of convex ice−water interface. The radius of the convex interface decreases with the decrease of temperature, as can be rationalized from the figures. The results, therefore, demonstrate that ice growth is inhibited by the formation of convex interface whose radius decreases with decrease in temperature below T_m. This is also predicted by eq 1 and hence the growth inhibition of ice by *Tm*AFP occurs according to the Kelvin effect. The starting configuration of S3 simulation was the final configuration of S1 simulation. So, S3 simulation was started with a preformed convex ice−water interface. The interface was formed at 220 K, lower than the temperature of S3 simulation (230 K). The interface will, therefore, start to melt as simulation progresses at 230 K because, according to eq 1, the critical radius of the interface will be larger at the reduced degree of supercooling. This indeed occurs, as evident from Figure 6. The interface continues to melt up to 25 ns. Then, no notable melting was observed during the rest of the time. So, the melting is inhibited. Importantly, the low-intensity region just beneath the reference plane persists in the distributions from 25 ns onward. However, no low-intensity region just beneath the reference plane was observed in the distributions at 220 and 225 K (Figures 4 and 5). Such low-intensity region just beneath the reference plane reveals the concave nature of the newly formed interface inward to ice phase. Temperature of S3 simulation is above the T_m of the water model. Therefore, the protein inhibits the melting of ice above the T_m with the formation of a concave interface between the adsorbed protein molecules. Such type of interface formation is also predicted by eq 1. Our simulations, therefore, completely agree with the predicted adsorption-inhibition mechanism for the ice growth inhibition and ice melting inhibition below and above T_m, respectively. Growth inhibition is accomplished with the formation of convex interface toward the liquid phase, and melting inhibition is accomplished with the formation of a concave interface inward the ice phase. To check the quantitative agreement of our results, we have estimated the radius of curvature of the curved surface formed in simulation and compared it to the value obtained from eq 1 at three temperatures. Radius is measured using the principle of spherometer[54] with rectangular base of dimension equal to that of the simulation cell in *xy*-plane. Approximate heights of the surfaces measured from Figures 4−6 are found to be 16, 5, and −3 Å at 220, 225, and 230 K, respectively. To evaluate the radius from eq 1, the values

DOI: 10.1021/acs.jpcb.8b00846
J. Phys. Chem. B 2018, 122, 3079−3087

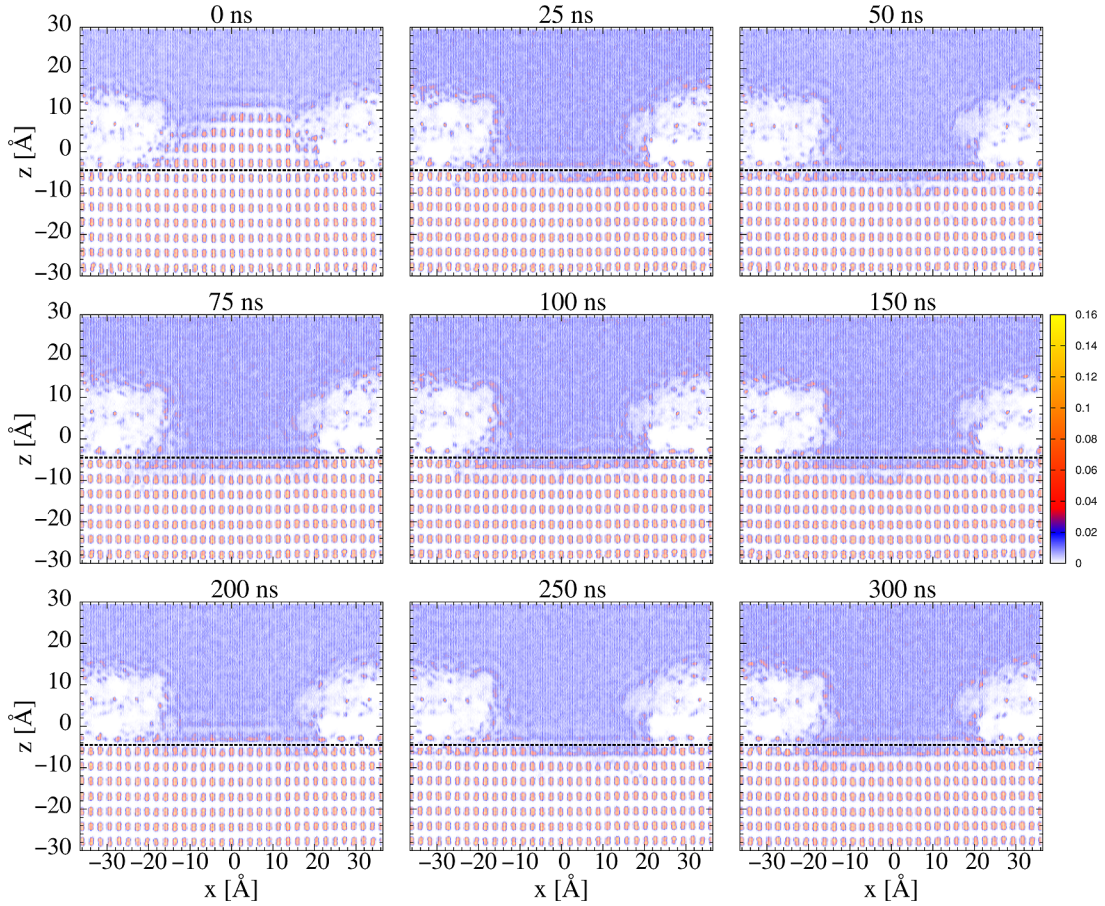

Figure 6. Two-dimensional probability distributions of water molecules around the *Tm*AFP protein on the *xz* plane (the protein helical axis is aligned along the *x* axis) as obtained at 0, 25, 50, 75, 100, 150, 200, 250, and 300 ns from simulation S3 at 230 K. In each panel, the reference plane, $z = -4$, is drawn as a black dashed line.

Table 2. Radius of Curvature (in Å) of the Surfaces as Obtained from Simulations S1 at 220 K, S2 at 225 K, and S3 at 230 K[a]

simulation	estimated value (from simulation)	theoretical value (from eq 1)
S1	72.33	54.34
S2	208.36	122.27
S3	−344.60	−489.09

[a]For comparison, the corresponding values as obtained from eq 1 are also included. The negative value represents the presence of concave interface inward to ice phase.

of σ and ΔH are taken from refs 45 and 55, respectively. The theoretical values along with those obtained from the simulations are listed in Table 2. It can be seen that simulation results are in good agreement with the values predicted by eq 1. This unequivocally proves that the inhibition obeys the Kelvin effect. Three-dimensional representations of the interfaces formed at three temperatures are displayed in Figure 7. It can be seen from the figure that the interface bulges toward liquid phase during growth inhibition and caves into ice phase during melting inhibition. We have not seen any curved step formation during the inhibition processes. It may be noted that we have continued the S1 simulation up to 500 ns, but no further change was observed. The melting simulation was also performed at two other temperatures, 233 and 235 K. At these temperatures, ice melted completely, but melting started from the uncovered area of the ice surface. Melting was not started just below the IBS of the protein, as seen by other simulations.[29,30] These studies showed that ice melts below the T_m of the water model. Such event does not appear in our simulations below T_m. The local melting below the T_m may be due to the absence of proper arrangement of the water molecules required for the binding of the protein with ice through its IBS. However, such melting cannot be precluded as the protein may come close to the ice surface without suitable interfacial water arrangement. Our simulations show that the growth is inhibited at a 10 K lower temperature than the T_m, whereas melting is inhibited at 1 K higher temperature than the T_m. This is because of the fact that the melting inhibition potential of AFPs is much less than the growth inhibition potential.[33] Because of such low potential, we were unable to repeat the melting inhibition simulation at a different temperature, whereas growth inhibition simulation was repeated at different temperatures.

4. CONCLUSIONS

In this article, we have presented results obtained from atomistic MD simulations of *Tm*AFP placed at the ice−water interface. Simulations are carried out below and above the equilibrium melting temperature of the employed water model. Attempts have been made to probe how the ice-bound protein inhibits the growth and melting of ice below and above the equilibrium melting temperature, respectively. The simulations show that below the melting temperature the protein allows

DOI: 10.1021/acs.jpcb.8b00846
J. Phys. Chem. B 2018, 122, 3079−3087

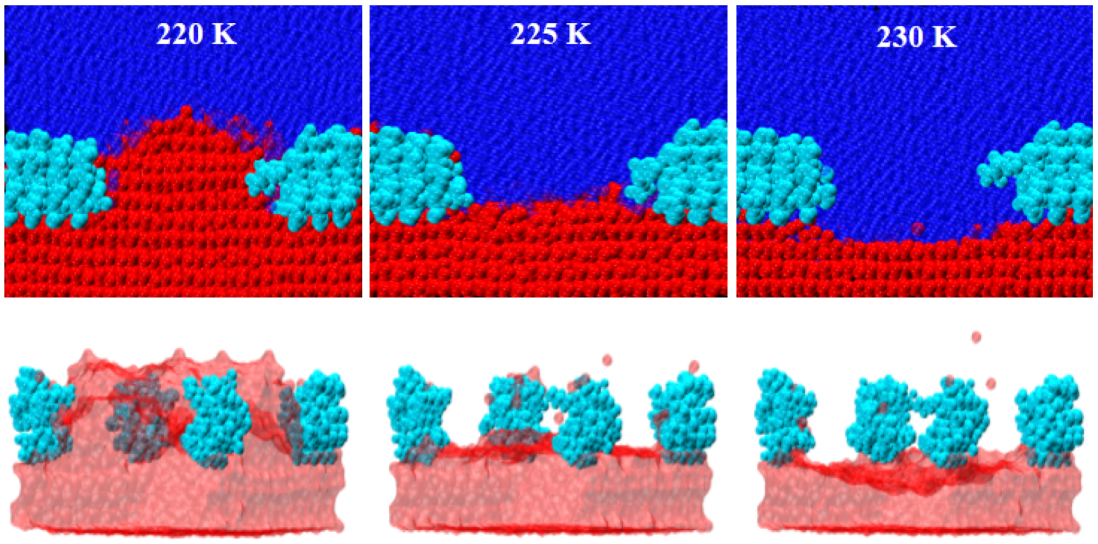

Figure 7. (Top) The nature of the ice−water interfaces formed in simulations S1 at 220 K, S2 at 225 K, and S3 at 230 K. Parts of the protein and its first virtual image along +*x* direction are drawn as the cyan spheres. Ice water molecules are shown by the red balls, and liquid water molecules are shown by the blue balls. Note that the interfaces formed at 220 and 225 K bulge toward liquid phase and the interface formed at 230 K caves into ice phase. (Bottom) Another view of the respective ice surfaces (red), where liquid water is not shown.

initial ice growth on the uncovered ice surface to form convex ice−water interface. After the formation of convex interface, ice growth is inhibited. The radius of the interface thus formed is found to be higher at low degree of supercooling (i.e., at higher temperature) and lower at high degree of supercooling (i.e., at lower temperature). We have seen the convex interface formation by local ice growth but not by local ice melting as obtained in earlier simulations.[29,30] Local growth-induced convex interface formation is originally predicted by the Kelvin effect. Such way of interface formation is also shown in recent simulation studies.[55] Our calculations further reveal that above the melting temperature the ice melting is inhibited through the formation of concave ice−water interface. These types of results are proposed to be obtained by the Kelvin effect, although its operation was verified little. Our results therefore clearly demonstrate its existence in the action of AFPs.

AUTHOR INFORMATION

Corresponding Author

*E-mail: sanjoy@chem.iitkgp.ernet.in. Phone: +91 3222 283344. Fax: +91 3222 255303.

ORCID

Sanjoy Bandyopadhyay: 0000-0002-3267-6326

Notes

The authors declare no competing financial interest.

ACKNOWLEDGMENTS

This study was supported by grants from the Department of Science and Technology (DST), Government of India, under the DST-FIST programme and the DST-IYC award. U.S.M. acknowledges the Council for Scientific and Industrial Research (CSIR), New Delhi, for providing scholarship.

REFERENCES

(1) Fletcher, G. L.; Hew, C. L.; Davies, P. L. Antifreeze Proteins of Teleost Fishes. *Annu. Rev. Physiol.* **2001**, *63*, 359−390.

(2) Graether, S. P.; Sykes, B. D. Cold Survival in Freeze-Intolerant Insects: The Structure and Function of *β*-Helical Antifreeze Proteins. *Eur. J. Biochem.* **2004**, *271*, 3285−3296.

(3) Griffith, M.; Yaish, M. W. Antifreeze Proteins in Overwintering Plants: A Tale of Two Activities. *Trends Plant Sci.* **2004**, *9*, 399−405.

(4) Gilbert, J. A.; Hill, P. J.; Dodd, C. E.; Laybourn-Parry, J. Demonstration of Antifreeze Protein Activity in Antarctic Lake Bacteria. *Microbiology* **2004**, *150*, 171−180.

(5) DeVries, A. L.; Wohlschlag, D. E. Freezing Resistance in Some Antarctic Fishes. *Science* **1969**, *163*, 1073−1075.

(6) Sicheri, F.; Yang, D. Ice-Binding Structure and Mechanism of an Antifreeze Protein from Winter Flounder. *Nature* **1995**, *375*, 427−431.

(7) Scotter, A. J.; Marshall, C. B.; Graham, L. A.; Gilbert, J. A.; Garnham, C. P.; Davies, P. L. The Basis for Hyperactivity of Antifreeze Proteins. *Cryobiology* **2006**, *53*, 229−239.

(8) Liou, Y.-C.; Tocilj, A.; Davies, P. L.; Jia, Z. Mimicry of Ice Structure by Surface Hydroxyls and Water of a *β*-Helix Antifreeze Protein. *Nature* **2000**, *406*, 322−324.

(9) Graether, S. P.; Kuiper, M. J.; Gagne, S. M.; Walker, V. K.; Jia, Z.; Sykes, B. D.; Davies, P. L. *β*-Helix Structure and Ice-Binding Properties of a Hyperactive Antifreeze Protein from an Insect. *Nature* **2000**, *406*, 325−328.

(10) Burcham, T. S.; Osuga, D.; Yeh, Y.; Feeney, R. A Kinetic Description of Antifreeze Glycoprotein Activity. *J. Biol. Chem.* **1986**, *261*, 6390−6397.

(11) Li, Q.; Luo, L. The Kinetic Theory of Thermal Hysteresis of a Macromolecule Solution. *Chem. Phys. Lett.* **1993**, *216*, 453−457.

(12) Wilson, P. A Model for Thermal Hysteresis Utilizing the Anisotropic Interfacial Energy of Ice Crystals. *Cryobiology* **1994**, *31*, 406−412.

(13) Hall, D. G.; Lips, A. Phenomenology and Mechanism of Antifreeze Peptide Activity. *Langmuir* **1999**, *15*, 1905−1912.

(14) Du, N.; Liu, X. Y.; Hew, C. L. Ice Nucleation Inhibition Mechanism of Antifreeze by Antifreeze Protein. *J. Biol. Chem.* **2003**, *278*, 36000−36004.

(15) Sander, L. M.; Tkachenko, A. V. Kinetic Pinning and Biological Antifreezes. *Phys. Rev. Lett.* **2004**, *93*, No. 128102.

(16) Anklam, M. R.; Firoozabadi, A. An Interfacial Energy Mechanism for the Complete Inhibition of Crystal Growth by Inhibitor Adsorption. *J. Chem. Phys.* **2005**, *123*, No. 144708.

(17) Raymond, J. A.; DeVries, A. L. Adsorption Inhibition as a Mechanism of Freezing Resistance in Polar Fishes. *Proc. Natl. Acad. Sci. U.S.A.* **1977**, *74*, 2589−2593.

(18) Knight, C. A.; Driggers, E.; DeVries, A. Adsorption to Ice of Fish Antifreeze Glycopeptides 7 and 8. *Biophys. J.* **1993**, *64*, 252.

DOI: 10.1021/acs.jpcb.8b00846
J. Phys. Chem. B 2018, 122, 3079−3087

(19) Knight, C. A.; Wierzbicki, A. Adsorption of Biomolecules to Ice and Their Effects upon Ice Growth. 2. A Discussion of the Basic Mechanism of "Antifreeze" Phenomena. *Cryst. Growth Des.* **2001**, *1*, 439−446.
(20) Zepeda, S.; Yokoyama, E.; Uda, Y.; Katagiri, C.; Furukawa, Y. In Situ Observation of Antifreeze Glycoprotein Kinetics at the Ice Interface Reveals a Two-Step Reversible Adsorption Mechanism. *Cryst. Growth Des.* **2008**, *8*, 3666−3672.
(21) Ba, Y.; Wongskhaluang, J.; Li, J. Reversible Binding of the HPLC6 Isoform of Type I Antifreeze Proteins to Ice Surfaces and the Antifreeze Mechanism Studied by Multiple Quantum Filtering-Spin Exchange NMR Experiment. *J. Am. Chem. Soc.* **2003**, *125*, 330−331.
(22) Pertaya, N.; Marshall, C. B.; DiPrinzio, C. L.; Wilen, L.; Thomson, E. S.; Wettlaufer, J.; Davies, P. L.; Braslavsky, I. Fluorescence Microscopy Evidence for Quasi-Permanent Attachment of Antifreeze Proteins to Ice Surfaces. *Biophys. J.* **2007**, *92*, 3663−3673.
(23) Celik, Y.; Drori, R.; Pertaya-Braun, N.; Altan, A.; Barton, T.; Bar-Dolev, M.; Groisman, A.; Davies, P. L.; Braslavsky, I. Microfluidic Experiments Reveal that Antifreeze Proteins Bound to Ice Crystals Suffice to Prevent Their Growth. *Proc. Natl. Acad. Sci. U.S.A.* **2013**, *110*, 1309−1314.
(24) Graham, L. A.; Liou, Y.-C.; Walker, V. K.; Davies, P. L. Hyperactive Antifreeze Protein from Beetles. *Nature* **1997**, *388*, 727−728.
(25) Wilson, P. W. Explaining Thermal Hysteresis by the Kelvin Effect. *CryoLetters* **1993**, *14*, 31−36.
(26) Wathen, B.; Kuiper, M.; Walker, V.; Jia, Z. A New Model for Simulating 3-D Crystal Growth and Its Application to the Study of Antifreeze Proteins. *J. Am. Chem. Soc.* **2003**, *125*, 729−737.
(27) Nada, H.; Furukawa, Y. Growth Inhibition Mechanism of an Ice-Water Interface by a Mutant of Winter Flounder Antifreeze Protein: A Molecular Dynamics Study. *J. Phys. Chem. B* **2008**, *112*, 7111−7119.
(28) Nada, H.; Furukawa, Y. Growth Inhibition at the Ice Prismatic Plane Induced by a Spruce Budworm Antifreeze Protein: A Molecular Dynamics Simulation Study. *Phys. Chem. Chem. Phys.* **2011**, *13*, 19936−19942.
(29) Calvaresi, M.; Hofinger, S.; Zerbetto, F. Local Ice Melting by an Antifreeze Protein. *Biomacromolecules* **2012**, *13*, 2046−2052.
(30) Todde, G.; Whitman, C.; Hovmöller, S.; Laaksonen, A. Induced Ice Melting by the Snow Flea Antifreeze Protein from Molecular Dynamics Simulations. *J. Phys. Chem. B* **2014**, *118*, 13527−13534.
(31) Kristiansen, E.; Zachariassen, K. E. The Mechanism by Which Fish Antifreeze Proteins Cause Thermal Hysteresis. *Cryobiology* **2005**, *51*, 262−280.
(32) Knight, C. A.; DeVries, A. Melting Inhibition and Superheating of Ice by an Antifreeze Glycopeptide. *Science* **1989**, *245*, 505−507.
(33) Celik, Y.; Graham, L. A.; Mok, Y.-F.; Bar, M.; Davies, P. L.; Braslavsky, I. Superheating of Ice Crystals in Antifreeze Protein Solutions. *Proc. Natl. Acad. Sci. U.S.A.* **2010**, *107*, 5423−5428.
(34) Cziko, P. A.; DeVries, A. L.; Evans, C. W.; Cheng, C.-H. C. Antifreeze Protein-Induced Superheating of Ice Inside Antarctic Notothenioid Fishes Inhibits Melting During Summer Warming. *Proc. Natl. Acad. Sci. U.S.A.* **2014**, *111*, 14583−14588.
(35) Midya, U. S.; Bandyopadhyay, S. Hydration Behavior at the Ice-Binding Surface of the *Tenebrio molitor* Antifreeze Protein. *J. Phys. Chem. B* **2014**, *118*, 4743−4752.
(36) Phillips, J. C.; Braun, R.; Wang, W.; Gumbart, J.; Tajkhorshid, E.; Villa, E.; Chipot, C.; Skeel, R. D.; Kale, L.; Schulten, K. Scalable Molecular Dynamics with NAMD. *J. Comput. Chem.* **2005**, *26*, 1781−1802.
(37) Bar-Dolev, M.; Celik, Y.; Wettlaufer, J. S.; Davies, P. L.; Braslavsky, I. New Insights into Ice Growth and Melting Modifications by Antifreeze Proteins. *J. R. Soc., Interface* **2012**, *9*, 3249−3259.
(38) Midya, U. S.; Bandyopadhyay, S. Interfacial Water Arrangement in the Ice-Bound State of an Antifreeze Protein: A Molecular Dynamics Simulation Study. *Langmuir* **2017**, *33*, 5499−5510.
(39) Allen, M. P.; Tildesley, D. J. *Computer Simulation of Liquids*; Oxford University Press, 1987.
(40) Ryckaert, J.-P.; Ciccotti, G.; Berendsen, H. J. Numerical Integration of the Cartesian Equations of Motion of a System with Constraints: Molecular Dynamics of N-Alkanes. *J. Comput. Phys.* **1977**, *23*, 327−341.
(41) Darden, T.; York, D.; Pedersen, L. Particle Mesh Ewald: An N·log(N) Method for Ewald Sums in Large Systems. *J. Chem. Phys.* **1993**, *98*, 10089−10092.
(42) MacKerell, A. D.; Bashford, D.; Bellott, M.; Dunbrack, R.; Evanseck, J.; Field, M. J.; Fischer, S.; Gao, J.; Guo, H.; Ha, S.; et al. All-Atom Empirical Potential for Molecular Modeling and Dynamics Studies of Proteins. *J. Phys. Chem. B* **1998**, *102*, 3586−3616.
(43) MacKerell, A. D., Jr.; Feig, M.; Brooks, C. L. Improved Treatment of the Protein Backbone in Empirical Force Fields. *J. Am. Chem. Soc.* **2004**, *126*, 698−699.
(44) Jorgensen, W. L.; Chandrasekhar, J.; Madura, J. D.; Impey, R. W.; Klein, M. L. Comparison of Simple Potential Functions for Simulating Liquid Water. *J. Chem. Phys.* **1983**, *79*, 926−935.
(45) Vega, C.; Sanz, E.; Abascal, J. L. F. The Melting Temperature of the Most Common Models of Water. *J. Chem. Phys.* **2005**, *122*, No. 114507.
(46) Fernández, R. G.; Abascal, J. L. F.; Vega, C. The Melting Point of Ice I_h for Common Water Models Calculated from Direct Coexistence of the Solid-Liquid Interface. *J. Chem. Phys.* **2006**, *124*, No. 144506.
(47) Koyama, Y.; Tanaka, H.; Gao, G.; Zeng, X. C. Melting Points and Thermal Expansivities of Proton-Disordered Hexagonal Ice with Several Model Potentials. *J. Chem. Phys.* **2004**, *121*, 7926−7931.
(48) Wang, J.; Yoo, S.; Bai, J.; Morris, J. R.; Zeng, X. C. Melting Temperature of Ice I_h Calculated from Coexisting Solid-Liquid Phases. *J. Chem. Phys.* **2005**, *123*, No. 036101.
(49) Steinhardt, P. J.; Nelson, D. R.; Ronchetti, M. Bond-Orientational Order in Liquids and Glasses. *Phys. Rev. B* **1983**, *28*, 784−805.
(50) Lechner, W.; Dellago, C. Accurate Determination of Crystal Structures Based on Averaged Local Bond Order Parameters. *J. Chem. Phys.* **2008**, *129*, No. 114707.
(51) Reinhardt, A.; Doye, J. P.; Noya, E. G.; Vega, C. Local Order Parameters for Use in Driving Homogeneous Ice Nucleation with All-Atom Models of Water. *J. Chem. Phys.* **2012**, *137*, No. 194504.
(52) Ebbinghaus, S.; Meister, K.; Prigozhin, M. B.; DeVries, A. L.; Havenith, M.; Dzubiella, J.; Gruebele, M. Functional Importance of Short-Range Binding and Long-Range Solvent Interactions in Helical Antifreeze Peptides. *Biophys. J.* **2012**, *103*, L20−L22.
(53) Meister, K.; Ebbinghaus, S.; Xu, Y.; Duman, J. G.; DeVries, A.; Gruebele, M.; Leitner, D. M.; Havenith, M. Long-Range Protein-Water Dynamics in Hyperactive Insect Antifreeze Proteins. *Proc. Natl. Acad. Sci. U.S.A.* **2013**, *110*, 1617−1622.
(54) Twyman, F. *Prism and Lens Making: A Textbook for Optical Glassworkers*; CRC Press, 1988.
(55) Kuiper, M. J.; Morton, C. J.; Abraham, S. E.; Gray-Weale, A. The Biological Function of an Insect Antifreeze Protein Simulated by Molecular Dynamics. *eLife* **2015**, *4*, No. e05142.

DOI: 10.1021/acs.jpcb.8b00846
J. Phys. Chem. B 2018, 122, 3079−3087